物理学报 Acta Physica Sinica
Chinese Physical Society
Institute of Physics, CAS

各向异性界面动力学与各向异性表面张力的相互作用对定向凝固过程中深胞晶生长的影响

蒋晗　陈明文　王涛　王自东

Effects of anisotropic interface kinetics and surface tension on deep cellular crystal growth in directional solidification

Jiang Han　Chen Ming-Wen　Wang Tao　Wang Zi-Dong

引用信息 Citation: Acta Physica Sinica, 66, 106801 (2017)　DOI: 10.7498/aps.66.106801
在线阅读 View online: http://dx.doi.org/10.7498/aps.66.106801
当期内容 View table of contents: http://wulixb.iphy.ac.cn/CN/Y2017/V66/I10

各向异性界面动力学与各向异性表面张力的相互作用对定向凝固过程中深胞晶生长的影响

蒋晗[1)] 陈明文[2)†] 王涛[1)] 王自东[1)‡]

1) (北京科技大学材料科学与工程学院, 北京 100083)

2) (北京科技大学数理学院, 北京 100083)

(2017 年 1 月 5 日收到; 2017 年 2 月 26 日收到修改稿)

通过应用匹配渐近展开法和多变量展开法研究了各向异性界面动力学与各向异性表面张力的相互作用对定向凝固过程中深胞晶生长的影响. 结果表明: 当各向异性界面动力学与各向异性表面张力的偏好方向之间相差角度为θ_0时, θ_0会对深胞晶生长形态产生影响; 当$0 \leqslant \theta_0 \leqslant \pi/4$时, 随着$\theta_0$的增大, 深胞晶的指状界面全长减小, 深胞晶根部的深度减小, 根部附近界面的曲率减小, 而曲率半径增大; 当$\pi/4 \leqslant \theta_0 \leqslant \pi/2$时, 随着$\theta_0$的增大, 深胞晶的指状界面全长增大, 深胞晶根部的深度增大, 根部附近界面的曲率增大, 而曲率半径减小.

关键词: 定向凝固, 各向异性表面张力, 各向异性界面动力学, 深胞晶生长

PACS: 68.70.+w, 81.10.Aj, 81.30.Fb **DOI:** 10.7498/aps.66.106801

1 引 言

几十年来, 定向凝固过程中的深胞晶生长一直是凝聚态物理和材料科学的研究重点. 已经有许多实验和数值模拟[1−4]通过使用Hele-Shaw模型对深胞晶生长问题进行了研究. Hele-Shaw模型包括细长的样本材料及两个恒温区: 一个高于平直界面液化温度T_M的高温区(温度为$T_{\rm H}$)和一个低于T_M的低温区(温度为$T_{\rm C}$). 以恒定速度V由高温区向低温区拉动样本, 随着拉速V的增加, 固液界面由低速生长的平直界面依次演变为小振幅的胞晶界面、大振幅的深胞晶界面、枝晶界面、细胞晶界面, 最后变为高速生长的平直界面. Xu等[5,6]在Mullins和Sekerka[7,8]建立的平界面形态线性稳定性理论(称为M-S理论)基础上, 运用Saffmen-Taylor[9]曲线坐标得到了各向同性表面张力下的深胞晶形态的近似解析解. 大量的研究表明, 各向异性表面张力和各向异性界面动力学都会对胞晶生长的界面形态产生影响. Etsuro和Sekerka[10]发现各向异性表面张力和各向异性界面动力学是胞晶生长存在优选方向的根本原因. 王志军等[11,12]和Trivedi等[13]分别研究了各向异性表面张力和各向异性界面动力学对定向凝固过程中胞晶微结构生长方向的影响, 发现各向异性表面张力和各向异性界面动力学都会使胞晶界面倾斜生长. 陈明文等[14,15]研究了考虑表面张力和界面动力学各向异性的定向凝固过程中深胞晶生长的界面形态, 揭示了深胞晶界面微结构形态形成的物理机制. 本文研究了各向异性表面张力和各向异性界面动力学的相互作用对深胞晶生长形态的影响, 即各向异性表面张力和各向异性界面动力学的偏好方向不一致, 相差角度为θ_0时, θ_0会对深胞晶生长形态产生影响.

2 定向凝固系统的数学模型

考虑定向凝固过程中的样本材料是细长的深胞晶生长, 凝固过程可视为二维. 且二元混合系统

† 通信作者. E-mail: chenmw@ustb.edu.cn

‡ 通信作者. E-mail: wangzd@mater.ustb.edu.cn

中的次组元为稀释的杂质; 忽略固相内的溶质扩散; 除扩散系数外的热力学性质在固相和液相内是相同的, 系统不存在对流. 该系统下的深胞晶生长, 其液相位于上半空间, 界面拉伸速度为V, 方向指向为液相方向向上. 界面随着时间的变化向上移动, 设原点位于胞晶尖端的直角坐标系Oxy中, 温度梯度为$G_{\rm T}$, 远场浓度为C_∞, 胞晶列的周期为$l_{\rm w}$.

选取深胞晶尖端曲率半径$l_{\rm t}$为长度尺度, $l_{\rm D}=\kappa_{\rm D}/V$为溶质扩散长度, 其中$\kappa_{\rm D}$为溶质扩散系数. 本文假定深胞晶尖端曲率半径远远小于溶质扩散长度, 即$l_{\rm t}\ll l_{\rm D}$. 选取Péclet数$Pe=\varepsilon=l_{\rm t}/l_{\rm D}$为小参数, 拉速$V$为速度尺度, $l_{\rm t}/V$为时间尺度, $\Delta H/(c_{\rm p}\rho)$为温度尺度, 其中ΔH为单位体积内固相产生的潜热, $c_{\rm p}$为液相比热, ρ为熔体密度, 远场浓度C_∞为浓度尺度. 于是, 热传导方程、溶质扩散方程和界面上的界面方程转化为无量纲的控制方程.

本文选取以下无量纲参数: $\Gamma=l_{\rm c}/l_{\rm t}$为表面张力参数且$\Gamma\ll1$, 其中$l_{\rm c}=\gamma c_{\rm p}\rho T_M/(\Delta H)^2$为毛细管长度, γ为表面张力系数; $M_*=V/\mu T_M$为界面动力学参数且$M_*\ll1$, 其中μ为界面动力学系数; $M=-\dfrac{mC_\infty}{\Delta H/(c_{\rm p}\rho)}$为形态学参数, 其中$m<0$是相图中液相线的斜率; $G=\dfrac{l_{\rm D}}{\Delta H/(c_{\rm p}\rho)}G_{\rm T}$为温度的无量纲梯度, $\lambda_{\rm G}=l_{\rm D}/l_{\rm G}=G/M$为两个长度单位之比, 其中$l_{\rm G}=-mC_\infty/G_{\rm T}$, $W=l_{\rm w}/l_{\rm t}$为主间距参数. 与文献[5]类似, 假设$\varepsilon\ll1$且$\Gamma=O(\varepsilon^2)$, $M_*=O(\varepsilon^2)$, 即$\Gamma=\varepsilon^2\hat{\Gamma}$, $M_*=\varepsilon^2m_*$, 这里$\hat{\Gamma}=O(1)$, $m_*=O(1)$.

由于解具有周期性, 可以仅考虑单个胞晶, 且胞晶侧壁为$x=\pm W$, W为自由参数. 假定矩形坐标(x,y)的原点位于胞晶的尖端, 生长区域的温度分布近似为仅与y有关的线性函数, 为$T=\varepsilon G(y-y_0)$, 其中y_0为坐标原点到温度为液化温度$T_{\rm L}=0$的距离. 选用Saffmen-Taylor (ST)解[9]构造曲线坐标系(ξ,η). 将Hele-Shaw流的流函数和势函数用$\Psi=(X,Y)$和$\Phi=(X,Y)$表示, 且有

$$\xi=-\Psi,\quad \eta=\Phi,\quad \zeta=\xi+\eta{\rm i}.$$

Saffmen-Taylor解可以转化为

$$\begin{aligned}Z&=X+Y{\rm i}=Z(\zeta)\\&=\lambda_0\zeta+{\rm i}\frac{2(1-\lambda_0)}{\pi}\ln\cos\left(\frac{\pi\zeta}{2}\right).\end{aligned}$$

曲线坐标于直角坐标系的转化关系为

$$\begin{aligned}x&=WX(\xi,\eta)\\&=W\left[\xi-\frac{2(1-\lambda_0)}{\pi}\arctan\left(\frac{\sin(\pi\xi)}{{\rm e}^{\pi\eta}+\cos(\pi\xi)}\right)\right],\\y&=WY(\xi,\eta)\\&=W\left\{(2\lambda_0-1)\eta+\frac{(1-\lambda_0)}{\pi}\ln\left[\frac{1}{4}[({\rm e}^{\pi\eta}-1)^2\right.\right.\\&\quad\left.\left.+2{\rm e}^{\pi\eta}(1+\cos(\pi\xi))]\right]\right\},\end{aligned}\tag{1}$$

其中λ_0是渐近宽度系数.

考虑4重对称的晶体的表面张力系数

$$\gamma=\gamma_0[1-\alpha_4\cos(4\theta)],\tag{2}$$

其中γ_0是各向同性表面张力系数, α_4是各向异性表面张力系数, θ是界面法向量与Oy轴之间的夹角.

界面动力学系数

$$\mu=\mu_0[1+\beta_4\cos(4\theta)],\tag{3}$$

其中μ_0是各向同性界面动力学系数, β_4是各向异性界面动力学系数.

在Saffmen-Taylor曲线坐标系下

$$\begin{aligned}\tan\theta&=\frac{[\partial Y(\xi,\eta)/\partial\xi]}{[\partial X(\xi,\eta)/\partial\xi]},\\\cos(4\theta)&=8\cos^4\theta-8\cos^2\theta+1\\&=B_0+B_1\eta_{\rm B}+B_2\eta'_{\rm B},\end{aligned}$$

由(2)式, 各向异性的表面张力参数变为

$$\Gamma=\varepsilon^2\hat{\Gamma}[1-\alpha_4\cos(4\theta)],$$

则有

$$1-\alpha_4\cos(4\theta)=1-\alpha_4(B_0+B_1\eta_{\rm B}+B_2\eta'_{\rm B}),\tag{4}$$

其中

$$\begin{aligned}B_0(\xi)=&\frac{1}{H^2}[(1-4\lambda_0+8\lambda_0^3-4\lambda_0^4)\\&-2(1-4\lambda_0+6\lambda_0^2-4\lambda_0^3)\cos(\pi\xi)\\&+(1-4\lambda_0+12\lambda_0^2-16\lambda_0^3+8\lambda_0^4)\\&\times\cos^2(\pi\xi)],\\B_1(\xi)=&-\frac{1}{H^3}[16\lambda_0\pi(1-\lambda_0)^3(\cos(\pi\xi)-1)\\&\times((2\lambda_0^2-2\lambda_0+1)\cos(\pi\xi)+(2\lambda_0-1))],\\B_2(\xi)=&\frac{1}{H^2}[16\lambda_0\pi(1-\lambda_0)\sin(\pi\xi)\\&\times((2\lambda_0^2-2\lambda_0+1)\cos(\pi\xi)+(2\lambda_0-1))],\\H=&(2\lambda_0-1)\cos(\pi\xi)+(2\lambda_0^2-2\lambda_0+1).\end{aligned}$$

由(3)式, 各向异性的界面动力学参数变为

$$M_* = \varepsilon^2 m_* \frac{1}{1+\beta_4\cos(4\theta)},$$

则有

$$\frac{1}{1+\beta_4\cos(4\theta)} = M_0 + M_1\eta_{\rm B} + M_2\eta'_{\rm B}, \tag{5}$$

其中

$$\begin{aligned}
M_0(\xi) =& \frac{1}{H_*}[(2\lambda_0^2-2\lambda_0+1)+(2\lambda_0-1)\cos(\pi\xi)]^2,\\
M_1(\xi) =& \frac{16}{H_*^2}\lambda_0\pi\beta_4(1-\lambda_0)^3(\cos(\pi\xi)-1)\\
&\times[(2\lambda_0^2-2\lambda_0+1)\cos(\pi\xi)+(2\lambda_0-1)]\\
&\times[(2\lambda_0^2-2\lambda_0+1)+(2\lambda_0-1)\cos(\pi\xi)],\\
M_2(\xi) =& -\frac{16}{H_*^2}\lambda_0\beta_4(1-\lambda_0)\sin(\pi\xi)\\
&\times[(2\lambda_0^2-2\lambda_0+1)\cos(\pi\xi)+(2\lambda_0-1)]\\
&\times[(2\lambda_0^2-2\lambda_0+1)+(2\lambda_0-1)\cos(\pi\xi)]^2,\\
H_*(\xi) =& [(1-4\lambda_0+8\lambda_0^2-8\lambda_0^3+4\lambda_0^4)\\
&+(1-4\lambda_0+8\lambda_0^3-4\lambda_0^4)\beta_4]\\
&-2[(1-4\lambda_0+6\lambda_0^2-4\lambda_0^3)\\
&+(1-4\lambda_0+6\lambda_0^2-4\lambda_0^3)\beta_4]\cos(\pi\xi)\\
&+[(1-4\lambda_0+4\lambda_0^2)\\
&+(1-4\lambda_0+12\lambda_0^2-16\lambda_0^3+8\lambda_0^4)\beta_4]\\
&\times\cos^2(\pi\xi).
\end{aligned}$$

当各向异性表面张力和各向异性界面动力学的偏好方向之间相差角度为θ_0时, 表面张力系数可以表示为[16]

$$\gamma = \gamma_0\{1-\alpha_4\cos[4(\theta-\theta_0)]\}.$$

由于

$$\begin{aligned}
&\cos[4(\theta-\theta_0)]\\
=&\cos(4\theta)\cos(4\theta_0)+\sin(4\theta)\sin(4\theta_0)\\
=&B_0+B_1\eta_{\rm B}+B_2\eta'_{\rm B},
\end{aligned}$$

则$B_0(\xi)$, $B_1(\xi)$, $B_2(\xi)$变为

$$\begin{aligned}
B_0(\xi) =& \frac{\cos(4\theta_0)}{H^2}[(1-4\lambda_0+8\lambda_0^3-4\lambda_0^4)\\
&-2(1-4\lambda_0+6\lambda_0^2-4\lambda_0^3)\cos(\pi\xi)\\
&+(1-4\lambda_0+12\lambda_0^2-16\lambda_0^3+8\lambda_0^4)\cos^2(\pi\xi)]\\
&+\frac{\sin(4\theta_0)}{H^2}\{4\lambda_0\sin(\pi\xi)(1-\lambda_0)[(2\lambda_0-1)\\
&-(2\lambda_0-1)\cos(\pi\xi)+2\lambda_0^2\cos^2(\pi\xi)]\},\\
B_1(\xi) =& -\frac{\cos(4\theta_0)}{H^3}\{16\lambda_0\pi(1-\lambda_0)^3[\cos(\pi\xi)-1]\\
&\times[(2\lambda_0^2-2\lambda_0+1)\cos(\pi\xi)+(2\lambda_0-1)]\}\\
&-\frac{\sin(4\theta_0)}{H^3}\frac{4\pi(\lambda_0-1)^2\sin(\pi\xi)}{\cos(\pi\xi)+1}\\
&\times[(-4\lambda_0^4+8\lambda_0^3-4\lambda_0+1)\\
&+(8\lambda_0^3-12\lambda_0^2+8\lambda_0-2)\cos(\pi\xi)\\
&+(8\lambda_0^4-16\lambda_0^3+12\lambda_0^2-4\lambda_0+1)\cos^2(\pi\xi)],\\
B_2(\xi) =& \frac{\cos(4\theta_0)}{H^2}\{16\lambda_0\pi(1-\lambda_0)\sin(\pi\xi)\\
&\times[(2\lambda_0^2-2\lambda_0+1)\cos(\pi\xi)+(2\lambda_0-1)]\}\\
&-\frac{\sin(4\theta_0)}{H^2}[(4-16\lambda_0+32\lambda_0^3-16\lambda_0^4)\\
&+(-8+32\lambda_0-48\lambda_0^2+32\lambda_0^3)\cos(\pi\xi)\\
&+(4-16\lambda_0+48\lambda_0^2-64\lambda_0^3+32\lambda_0^4)\\
&\times\cos^2(\pi\xi)].
\end{aligned}$$

在曲线坐标系(ξ,η)下, 整个物理空间被分为远离根部的外部区域和根部附近的内部区域.

深胞晶生长的稳态解$(C,\eta_{\rm B})$满足控制方程

$$\frac{\partial^2 C}{\partial\xi^2}+\frac{\partial^2 C}{\partial\eta^2}+\varepsilon W\left(Y_\xi\frac{\partial C}{\partial\xi}+X_\xi\frac{\partial C}{\partial\eta}\right)=0 \tag{6}$$

和边界条件: 在远离根部底端区域的外部区域($\lfloor\xi\rfloor\leqslant 1$, $|\eta_{\rm B}|\ll 1$)的界面上, 界面条件可以在$\eta=0$处泰勒展开, 且界面的局部速度$U_{\rm I}$为

$$U_{\rm I} = \frac{Y_\eta(\xi,0)+Y_{\eta\eta}(\xi,0)\eta_{\rm B}-Y_\xi(\xi,0)\hat{\eta'}_{\rm B}}{G_0(\xi,0)}, \tag{7}$$

则Gibbs-Thomson条件为

$$\begin{aligned}
&C(\xi,0)+\frac{\partial C(\xi,0)}{\partial\eta}\eta_{\rm B}+\cdots\\
=&\, y_* - \varepsilon\lambda_{\rm G}W(Y(\xi,0)+Y_\eta(\xi,0)\eta_{\rm B})\\
&-\frac{\varepsilon^2\hat{\Gamma}}{MW}\left[K_{0,0}(1-\alpha_4B_0-\alpha_4B_1\eta_{\rm B}-\alpha_4B_2\eta'_{\rm B})\right.\\
&\left.-\frac{1}{G_0}\frac{\partial^2\eta_{\rm B}}{d\xi^2}(1-\alpha_4B_0-\alpha_4B_1\eta_{\rm B}-\alpha_4B_2\eta'_{\rm B})\right]\\
&-\frac{\varepsilon^2E^{-1}m_*}{M}(M_0(\xi)+M_1(\xi)\eta_{\rm B}+M_2(\xi)\eta'_{\rm B})U_{\rm I}\\
&+O(\text{h.o.t}),
\end{aligned} \tag{8}$$

质量守恒条件为

$$\begin{aligned}
&\frac{\partial C(\xi,0)}{\partial\eta}+\frac{\partial^2C(\xi,0)}{\partial\eta^2}\eta_{\rm B}-\eta'_{\rm B}\frac{\partial C(\xi,0)}{\partial\xi}\\
&-\varepsilon W(1-\kappa)\times\left[C(\xi,0)+\frac{\partial C(\xi,0)}{\partial\eta}\eta_{\rm B}\right]\\
&\times[Y_\xi(\xi,0)\eta'_{\rm B}-Y_\eta(\xi,0)-Y_{\eta\eta}(\xi,0)\eta_{\rm B}]\\
&+O(\text{h.o.t})=0,
\end{aligned} \tag{9}$$

其中 κ 为分离系数, $O(\text{h.o.t})$ 为高阶项,

$$y_* = \varepsilon\lambda_{\rm G} y_0, \quad E = \Delta H/c_{\rm P}\rho T_{M0},$$
$$K_{0,0}(\xi) = \frac{\pi\lambda_0(1-\lambda_0)}{G_0^3[1+\cos(\pi\xi)]},$$
$$G_0(\xi) = \left[\lambda_0^2 + (1-\lambda_0)^2 tg^2\frac{\pi\xi}{2}\right]^{1/2}.$$

在胞晶尖端, 当 $\xi=\eta=0$ 时,

$$\frac{\partial\eta_{\rm B}}{\partial\xi}(0) = \eta_{\rm B}(0) = 0. \tag{10}$$

在根部底端, 当 $\xi=\pm1$, $\eta=\eta_{\rm b}$ 时,

$$\eta_{\rm B}(\pm1) = \eta_{\rm b}, \quad \frac{\partial\eta_{\rm B}}{\partial\xi}(\pm1) = 0. \tag{11}$$

在胞晶侧壁, 当 $\xi=\pm1$ 时,

$$\frac{\partial C}{\partial\xi}(\pm1,\eta) = 0. \tag{12}$$

在远场处, 当 $\eta\to\infty$ 时,

$$C \sim 1 + Q_0\,{\rm e}^{-\varepsilon W\eta}, \tag{13}$$

其中 Q_0 是与变量 ξ 和 η 无关的常数.

3 外部区域的渐近解

控制方程 (6), 界面条件 (8) 和 (9), 尖端光滑条件 (10), 侧壁条件 (12) 和远场条件 (13) 组成了一个非齐次的外部系统, 该非齐次系统有如下形式的解 [5]:

$$\{C,\eta_{\rm B}\} = \{\bar{C},\bar{\eta}_{\rm B}\} + \{\tilde{C},\tilde{\eta}_{\rm B}\}, \tag{14}$$

(14) 式中的 $\bar{C}(\xi,\eta,\varepsilon)$, $\bar{\eta}_{\rm B}(\xi,\varepsilon)$ 部分是非齐次系统的一个特解, $\tilde{C}(\xi,\eta,\varepsilon)$, $\tilde{\eta}_{\rm B}(\xi,\varepsilon)$ 部分是相应的齐次系统的通解.

运用文献 [5] 中的方法得到 (14) 式中非齐次系统的渐近解为

$$\begin{aligned}\bar{C} = {}& 1 + (y_{*0}-1)\,{\rm e}^{-W\tilde{\eta}} + \varepsilon[y_{*1}\,{\rm e}^{-W\tilde{\eta}} \\ & + W\lambda_{\rm G}\tau_0(1-{\rm e}^{-W\tilde{\eta}}) \\ & - W\lambda_{\rm G}Y(\xi,\eta) + W\lambda_{\rm G}\eta],\end{aligned}$$
$$\bar{\eta}_{\rm B}(\xi,\varepsilon) = \varepsilon\eta_1(\xi) = \varepsilon\sum_{m=0}^{\infty} B_{1,m}\cos(m\pi\xi), \tag{15}$$

其中

$$y_{*0} = \frac{1+\lambda_{\rm G}(1-\lambda_0)}{1-\lambda_0(1-\kappa)},$$
$$\begin{aligned}y_{*1} = {}& \frac{\tau_0 W}{2[(1-\kappa)\lambda_0-1]}\Big\{y_{*0}-1-\lambda_{\rm G} \\ & + \lambda_0\lambda_{\rm G}\left[(1-\kappa)\left(2-\frac{y_{*0}}{\lambda_{\rm G}}\right)-1\right]\Big\},\end{aligned}$$
$$\tau_0 = \frac{-(2\ln 2)(1-\lambda_0)}{\pi}, \quad W = \frac{\pi(1-\lambda_0)}{2\lambda_0^2},$$
$$\begin{aligned}&\left(\sum_{n=0}^{\infty}\hat{Q}_{m,n} - \frac{\lambda_0}{1-\lambda_0}\right)B_{1,m} \\ &= \frac{\lambda_0}{W\Delta_0(1-\lambda_0)}\times\left[W^2(1-\kappa)\frac{\lambda_0\lambda_{\rm G}}{m\pi}\tau_m\right. \\ &\quad - \frac{\hat{\Gamma}}{MW}\gamma_m - E_{2,m}(0,0) \\ &\quad - \frac{1}{m\pi}\frac{\partial E_{2,m}(0,0)}{\partial\eta} + \frac{\hat{\Gamma}}{MW}\alpha_4 s_m \\ &\quad \left. - \frac{E^{-1}m_*}{M}L_m\right],\end{aligned}$$
$$s_m = \int_{-1}^{1} K_{0,0}(\xi)B_0(\xi)\cos(m\pi\xi)\,{\rm d}\xi, L_m$$
$$= \int_{-1}^{1}\frac{\lambda_0 M_0(\xi)}{G_0(\xi)}\cos(m\pi\xi)\,{\rm d}\xi,$$
$$\gamma_m = \int_{-1}^{1} K_{0,0}(\xi)\cos(m\pi\xi)\,{\rm d}\xi,$$
$$\tau_m = \int_{-1}^{1} Y(\xi,0)\cos(m\pi\xi)\,{\rm d}\xi,$$
$$E_{2,m}(0,0) = \int_{-1}^{1}\frac{1}{2}W_0^2\lambda_{\rm G}Y^2(\xi,0)\cos(m\pi\xi)\,{\rm d}\xi,$$
$$\begin{aligned}&\frac{\partial E_{2,m}(0,0)}{\partial\eta} \\ &= \int_{-1}^{1}\frac{1}{2}W_0^2\lambda_0[(1-\kappa)y_{*0}+\lambda_{\rm G}]Y(\xi,0) \\ &\quad \times\cos(m\pi\xi)\,{\rm d}\xi,\end{aligned}$$
$$\Delta_0 = \lambda_0[(1-\kappa)y_{*0} - \lambda_{\rm G}],$$
$$\hat{Q}_{m,n} = \begin{cases}0 & (n>m)\\ (-1)^{m+n+1}2 & (n<m)\\ -1 & (n=m)\end{cases}.$$

(14) 式中齐次系统的通解为

$$\begin{aligned}&\tilde{C}_{*0}(\xi,\xi_+,0,0) \\ &= -\eta(0)W\Delta_0\frac{1}{\lambda_0}\frac{\partial Y(\xi,0)}{\partial\xi}\,{\rm e}^{-\frac{\chi_{\rm I}(\xi)}{\sqrt{\varepsilon\hat{\Gamma}}}}\sin\frac{\chi_{\rm R}(\xi)}{\sqrt{\varepsilon\hat{\Gamma}}},\end{aligned}$$
$$\tilde{\eta}_{\rm B}(\xi,\varepsilon) = -\varepsilon\eta(0)\,{\rm e}^{\frac{\chi_{\rm I}(\xi)}{\sqrt{\varepsilon\hat{\Gamma}}}}\cos\frac{-\chi_{\rm R}(\xi)}{\sqrt{\varepsilon\hat{\Gamma}}}, \tag{16}$$

其中

$$\chi(\xi) = \int_0^{\xi} k_{\rm s}(\xi_1)\,{\rm d}\xi_1 = \chi_{\rm R}(\xi) + {\rm i}\chi_{\rm I}(\xi),$$
$$k_{\rm s}(\xi) = \sqrt{\frac{W^2\Delta_0 M G_0}{1-\alpha_4 B_0}\left[1+\frac{\rm i}{\lambda_0}\frac{\partial Y(\xi,0)}{\partial\xi}\right]}.$$

将 (15) 与 (16) 式进行匹配, 可以得到外解为

$$\begin{aligned} C(\xi,0) &= y_{*0}+\varepsilon[y_{*1}-W\lambda_{\rm G}Y(\xi,0)] \\ &\quad -\varepsilon^2\eta_1(0)W\Delta_0\frac{1}{\lambda_0}\frac{\partial Y(\xi,0)}{\partial\xi}\,{\rm e}^{-\frac{\chi_{\rm I}(\xi)}{\sqrt{\varepsilon\hat{\Gamma}}}} \\ &\quad \times\sin\frac{\chi_{\rm R}(\xi)}{\sqrt{\varepsilon\hat{\Gamma}}}+\cdots, \\ \eta_{\rm B}(\xi,\varepsilon) &= \varepsilon\eta_1(\xi)-\varepsilon\eta_1(0)\,{\rm e}^{\frac{\chi_{\rm I}(\xi)}{\sqrt{\varepsilon\hat{\Gamma}}}}\cos\frac{-\chi_{\rm R}(\xi)}{\sqrt{\varepsilon\hat{\Gamma}}}. \end{aligned} \tag{17}$$

4 根部区域的渐近解

由于外解 (17) 式在 $\xi=\pm1$ 处不满足根部光滑条件, 因此外解不能提供根部底端的位置, 需要求根部区域的内解. 当 $\xi\to-1$ 时, 由 (15) 式有

$$\eta_1(\xi)\sim c_0(1+\xi)^{\rm c}+\cdots,\quad 0<c<1, \tag{18}$$

且 $\eta_1'(-1)\to\infty$.

设 $\eta=\eta_{\rm T}(\xi)$ 为根部区域的中心线, 并且是根部区域界面形状函数的近似. 在根部区域 ($|\xi+1|\ll1$, $|\eta-\eta_{\rm T}(\xi)|\ll1$), 引入内部变量 $\hat{\xi}$ 和 $\hat{\eta}$ [5]:

$$\hat{\xi}=\frac{1+\xi}{\delta(\varepsilon)},\quad \hat{\eta}=\frac{\eta-\eta_{\rm T}}{\delta(\varepsilon)}. \tag{19}$$

由 (18) 式, 在根部区域的远场有

$$\eta_{\rm B}(\xi)\approx\varepsilon c_0(1+\xi)^{\rm c}, \tag{20}$$

为了与外解匹配, 根部的远场满足

$$\begin{aligned} \eta_{\rm T}(\xi) &= \varepsilon c_0(1+\xi)^{\rm c}=\varepsilon\delta^{\rm c}(\varepsilon)c_0\hat{\xi}^{\rm c} \\ &= \delta(\varepsilon)\hat{\eta}_{\rm T}(\hat{\xi}), \end{aligned} \tag{21}$$

则必须设 $\delta(\varepsilon)=\varepsilon\delta^{\rm c}(\varepsilon)$, 即 $\delta(\varepsilon)=\varepsilon^{\frac{1}{1-c}}$, $\hat{\eta}_{\rm T}(\hat{\xi})=c_0\hat{\xi}^{\rm c}$.

在根部底端 $\hat{\xi}=0$ 处, $\eta_{\rm B}(\xi)\approx\varepsilon c_0(1+\xi)^{\rm c}$ 违反了根部光滑条件 $\eta_{\rm T}'(0)=0$, 所以界面表达式可以写为 $\eta_{\rm B}(\xi)=\delta(\varepsilon)\hat{\eta}_{\rm T}(\hat{\xi})$, 且 $\hat{\eta}_{\rm T}(\hat{\xi})=\hat{\eta}_{\rm b}+c_2\hat{\xi}^2+c_3\hat{\xi}^3$. 为了描述界面形状函数 $\hat{\eta}_{\rm T}(\hat{\xi})$, 需要用一个内在过渡点 $0<\hat{\xi}_{\rm T}<\infty$ 将根部区域分为三个子区域, 并且在不同的子区域使用不同的形式来表示界面形状:

在子区域 I 内, 当 $\hat{\xi}_{\rm T}<\hat{\xi}<\infty$, $\hat{\eta}_{\rm T}^{(I)}(\hat{\xi})=c_0\hat{\xi}^{\rm c}+\cdots$;

在子区域 II 内, 当 $0\leqslant\hat{\xi}<\hat{\xi}_{\rm T}$, $\hat{\eta}_{\rm T}^{(II)}(\hat{\xi})=\delta(\varepsilon)[\hat{\eta}_{\rm b}+c_2\hat{\xi}^2+c_3\hat{\xi}^3]+\cdots$;

在子区域 III 内, 以 $\hat{\xi}_{\rm T}=\hat{\xi}$ 为中心并且连接子区域 I 和 II, 该子区域内从 $\hat{\eta}_{\rm T}^{(I)}(\hat{\xi})$ 过度为 $\hat{\eta}_{\rm T}^{(II)}(\hat{\xi})$.

为了满足匹配条件, 需要在 $\hat{\xi}\to\hat{\xi}_{\rm T}^{\pm}$ 处有

$$\hat{\eta}_{\rm T}^{(I)}(\hat{\xi}_{\rm T})=\hat{\eta}_{\rm T}^{(II)}(\hat{\xi}_{\rm T}), \tag{22}$$

且

$$\begin{aligned} &\frac{{\rm d}^k}{{\rm d}\hat{\xi}^k}\hat{\eta}_{\rm T}^{(I)}(\hat{\xi}_{\rm T})=\frac{{\rm d}^k}{{\rm d}\hat{\xi}^k}\hat{\eta}_{\rm T}^{(II)}(\hat{\xi}_{\rm T}) \\ &\qquad (k=1,2,\cdots), \end{aligned} \tag{23}$$

其中 $\hat{\xi}_{\rm T}$ 依赖参数 ε, 且有以下的渐近展开

$$\hat{\xi}_{\rm T}(\varepsilon)=\hat{\xi}_*(\varepsilon)[1+d_1\delta(\varepsilon)+\cdots],\quad(\varepsilon\to0), \tag{24}$$

因此, 在首级近似中,

$$\hat{\eta}_{\rm T}(\hat{\xi}) = \begin{cases} c_0\hat{\xi}^{\rm c} & ({\rm I}):(\hat{\xi}_*<\hat{\xi}<\infty) \\ \hat{\eta}_{\rm b}+c_2\hat{\xi}^2+c_3\hat{\xi}^3 & ({\rm II}):(0\leqslant\hat{\xi}<\hat{\xi}_{\rm T}) \end{cases}, \tag{25}$$

参数

$$\begin{aligned} &\hat{\eta}_*=c_0\hat{\xi}_*^{\rm c},\quad \hat{\eta}_{\rm b}=\left[1-\frac{c(5-c)}{6}\right]\hat{\xi}_*, \\ &c_2=\frac{c(3-c)\hat{\eta}_*}{2\hat{\xi}_*^2},\quad c_3=-\frac{c(2-c)\hat{\eta}_*}{3\hat{\xi}_*^3}, \end{aligned}$$

其中 $\hat{\xi}_*$ 是待定的特征值. 至此, 界面形状函数变为如下形式:

$$\eta_{\rm B}(\xi,\varepsilon)=\delta(\varepsilon)[\hat{\eta}_{\rm T}(\hat{\xi})+\hat{\eta}_{\rm B}(\hat{\xi},\varepsilon)+\cdots], \tag{26}$$

且在根部区域, $|\hat{\eta}_{\rm B}(\hat{\xi},\varepsilon)|\ll1$.

将坐标函数 (1) 在 $\eta\to0$, $\xi\to-1$ 做泰勒展开, 相应的参数变为

$$\begin{aligned} &R\sim\pi^2\delta^2(\varepsilon)(\hat{\eta}+\hat{\eta}_{\rm T})^2+\pi^2\delta^2(\varepsilon)\hat{\xi}^2+\cdots, \\ &\hat{Y}(\hat{\xi},\hat{\eta},\varepsilon)\sim\hat{Y}_*\ln\delta(\varepsilon)+\hat{Y}_0+\hat{Y}_1\delta(\varepsilon)+\cdots, \\ &\frac{\partial Y(\xi,\eta)}{\partial\eta}\sim\hat{Y}_{\hat{\eta},1}+\frac{1}{\delta(\varepsilon)}\hat{Y}_{\hat{\eta},0}+\cdots, \\ &\frac{\partial Y(\xi,\eta)}{\partial\xi}\sim\frac{1}{\delta(\varepsilon)}\hat{Y}_{\hat{\xi},0}+\cdots, \\ &\frac{\partial^2Y(\xi,\eta)}{\partial\eta^2}\sim\frac{1}{\delta^2(\varepsilon)}\hat{Y}_{\hat{\eta}\hat{\eta},0}+\cdots, \\ &G(\xi,\eta)\sim\frac{1}{\delta(\varepsilon)}\frac{2(1-\lambda_0)}{\pi}\frac{1}{\sqrt{(\hat{\eta}+\hat{\eta}_{\rm T})^2+\hat{\xi}^2}}, \\ &\hat{K}_{0,0}\sim\frac{\pi}{2(1-\lambda_0)}\frac{\hat{\eta}_{\rm T}}{\sqrt{\hat{\eta}_{\rm T}^2+\hat{\xi}^2}}, \\ &G_0\sim\frac{1}{\delta(\varepsilon)}\frac{2(1-\lambda_0)}{\pi}\frac{1}{\sqrt{\hat{\eta}_{\rm T}^2+\hat{\xi}^2}}, \end{aligned}$$

$$\hat{G}_0 \sim \frac{2(1-\lambda_0)}{\pi}\frac{1}{\sqrt{\hat{\eta}_{\rm T}^2+\hat{\xi}^2}},\ \hat{B}_0(\hat{\xi}) \sim \cos 4\theta_0,$$
$$\hat{B}_1(\hat{\xi}) \sim -\frac{8\pi\lambda_0}{1-\lambda_0}\cos 4\theta_0,\ \hat{B}_2(\hat{\xi}) \sim -4\cos 4\theta_0,$$
$$\hat{M}_0(\hat{\xi}) \sim \frac{1}{1+\beta_4},$$
$$\hat{M}_1(\hat{\xi}) \sim \frac{8\pi\lambda_0\beta_4}{(1-\lambda_0)(1+\beta_4)^2},$$
$$\hat{M}_2(\hat{\xi}) \sim 0,$$

其中

$$\hat{Y}_* = \frac{2(1-\lambda_0)}{\pi},$$
$$\hat{Y}_0 = \frac{(1-\lambda_0)}{\pi}\ln\left[\pi^2\frac{(\hat{\eta}+\hat{\eta}_{\rm T})^2+\hat{\xi}^2}{4}\right],$$
$$\hat{Y}_1 = \lambda_0(\hat{\eta}+\hat{\eta}_{\rm T}),$$
$$\hat{Y}_{\hat{\eta},0} = \frac{2(1-\lambda_0)}{\pi}\frac{\hat{\eta}+\hat{\eta}_{\rm T}}{(\hat{\eta}+\hat{\eta}_{\rm T})^2+\hat{\xi}^2},$$
$$\hat{Y}_{\hat{\eta},1} = \lambda_0,$$
$$\hat{Y}_{\hat{\xi},0} = \frac{2(1-\lambda_0)}{\pi}\frac{\hat{\xi}}{(\hat{\eta}+\hat{\eta}_{\rm T})^2+\hat{\xi}^2},$$
$$\hat{Y}_{\hat{\eta}\hat{\eta},0} = \frac{2(1-\lambda_0)}{\pi}\frac{1}{(\hat{\eta}+\hat{\eta}_{\rm T})^2+\hat{\xi}^2}.$$

在根部区域中使用内变量 $\{\hat{\xi},\hat{\eta}\}$, 浓度场变为 $C=\hat{C}(\hat{\xi},\hat{\eta},\varepsilon)$, 控制方程 (6) 变为

$$\frac{\partial^2\hat{C}}{\partial\hat{\xi}^2}+\left[1+\left(\frac{\partial\hat{\eta}_{\rm T}}{\partial\hat{\xi}}\right)^2\right]\frac{\partial^2\hat{C}}{\partial\hat{\eta}^2}-2\frac{\partial\hat{\eta}_{\rm T}}{\partial\hat{\xi}}\frac{\partial^2\hat{C}}{\partial\hat{\xi}\partial\hat{\eta}}$$
$$-\frac{\partial^2\hat{\eta}_{\rm T}}{\partial\hat{\xi}^2}\frac{\partial\hat{C}}{\partial\hat{\eta}}$$
$$+\varepsilon W\left[\hat{Y}_{\hat{\xi}}\left(\frac{\partial\hat{C}}{\partial\hat{\xi}}-\frac{\partial\hat{\eta}_{\rm T}}{\partial\hat{\xi}}\frac{\partial\hat{C}}{\partial\hat{\eta}}\right)+\hat{X}_{\hat{\xi}}\frac{\partial\hat{C}}{\partial\hat{\eta}}\right]$$
$$=0. \tag{27}$$

相应的界面条件 (8)—(13) 变为:

Gibbs-Thomson 条件

$$\hat{C}+\frac{\partial\hat{C}}{\partial\hat{\eta}}\hat{\eta}_{\rm B}$$
$$=y_*-\varepsilon\lambda_{\rm G}W(\hat{Y}_*\ln\delta(\varepsilon)+\hat{Y}_0+\hat{Y}_1\delta(\varepsilon)+\cdots)$$
$$-\varepsilon\lambda_{\rm G}W(\hat{Y}_{\hat{\eta},0}+\delta(\varepsilon)\hat{Y}_{\hat{\eta},1})\hat{\eta}_{\rm B}$$
$$-\frac{\varepsilon^2\hat{\Gamma}}{MW}\left[\hat{K}_{0,0}(1-\alpha_4\hat{B}_0-\alpha_4\hat{B}_1\delta(\varepsilon)\hat{\eta}_{\rm B}\right.$$
$$-\alpha_4\hat{B}_2\hat{\eta'}_{\rm B})-\frac{1}{\hat{G}_0}\frac{\partial^2\hat{\eta}_{\rm B}}{d\hat{\xi}^2}(1$$
$$\left.-\alpha_4\hat{B}_0-\alpha_4\hat{B}_1\delta(\varepsilon)\hat{\eta}_{\rm B}-\alpha_4\hat{B}_2\hat{\eta'}_{\rm B})\right]$$
$$-\frac{\varepsilon^2E^{-1}m_*}{M}[\hat{M}_0+\hat{M}_1\delta(\varepsilon)\hat{\eta}_{\rm B}+\hat{M}_2\hat{\eta'}_{\rm B}]$$
$$\times\left[\frac{\hat{Y}_{\hat{\eta}}+\hat{Y}_{\hat{\eta}\hat{\eta}}\hat{\eta}_{\rm B}-\hat{Y}_{\hat{\xi}}\hat{\eta'}_{\rm B}}{\hat{G}_0}\right]+O(\hat{\eta}_{\rm B}^2). \tag{28}$$

质量守恒条件

$$\frac{\partial\hat{C}}{\partial\hat{\eta}}+\frac{\partial^2\hat{C}}{\partial\hat{\eta}^2}\hat{\eta}_{\rm B}-\hat{\eta'}_{\rm B}\left(\frac{\partial\hat{C}}{\partial\hat{\xi}}-\hat{\eta}'_{\rm T}\frac{\partial\hat{C}}{\partial\hat{\eta}}\right)$$
$$-\varepsilon W(1-\kappa)\times\left[\hat{C}+\frac{\partial\hat{C}}{\partial\hat{\eta}}\hat{\eta}_{\rm B}\right]$$
$$\times[\hat{Y}_{\hat{\xi}}\hat{\eta'}_{\rm B}-\hat{Y}_{\hat{\eta}}-\hat{Y}_{\hat{\eta}\hat{\eta}}\hat{\eta}_{\rm B}]+O(\hat{\eta}_{\rm B}^2)=0. \tag{29}$$

在胞晶侧壁, 当 $\hat{\xi}=0$ 时,

$$\bar{C}_{S*0}(\hat{\xi},\hat{\eta},\tilde{\eta}_{\rm S})=\bar{C}_{S*0}(-\hat{\xi},\hat{\eta},\tilde{\eta}_{\rm S}). \tag{30}$$

在远场处, 当 $\hat{\xi}\to\infty$ 时,

$$\bar{C}_{S*}\Leftrightarrow\bar{C}_*. \tag{31}$$

上述非齐次系统 (27)—(31) 存在如下形式的解 [5]:

$$\hat{C}(\hat{\xi},\hat{\eta},\varepsilon)=\bar{C}_{\rm S}(\hat{\xi},\hat{\eta},\varepsilon)+\tilde{C}_{\rm S}(\hat{\xi},\hat{\eta},\varepsilon),$$
$$\hat{\eta}_{\rm B}(\hat{\xi},\varepsilon)=\bar{\eta}_{\rm S}(\hat{\xi},\varepsilon)+\tilde{\eta}_{\rm S}(\hat{\xi},\varepsilon), \tag{32}$$

(32) 式中的 $\bar{C}_{\rm S}(\hat{\xi},\hat{\eta},\varepsilon)$, $\bar{\eta}_{\rm S}(\hat{\xi},\varepsilon)$ 是非齐次系统的一个特解, $\tilde{C}_{\rm S}(\hat{\xi},\hat{\eta},\varepsilon)$, $\tilde{\eta}_{\rm S}(\hat{\xi},\varepsilon)$ 是相应的齐次系统的通解.

运用文献 [5] 中的方法可以得到 (32) 式中非齐次系统的渐近解为

$$\bar{C}_{S*}\sim y_{*0}-\varepsilon\ln\delta(\varepsilon)W\lambda_{\rm G}\hat{Y}_*$$
$$+\varepsilon[y_{*1}-W\lambda_{\rm G}\hat{Y}_0(\hat{\xi},\hat{\eta})]+({\rm h.o.t}), \tag{33}$$

相应的齐次系统的通解为

$$\hat{\eta}_{\rm B}(\xi,\varepsilon)=\delta(\varepsilon)\hat{\eta}_{\rm T}(\hat{\xi})-\varepsilon\eta_1(0)\Delta(\varepsilon)$$
$$\times\exp\left\{-\frac{\rm i}{\sqrt{\varepsilon\hat{\Gamma}}}\hat{\chi}(\hat{\xi})\right\}, \tag{34}$$

量子化条件为

$$q_n=\frac{W(1-\lambda_0)}{\pi\sqrt{\varepsilon\hat{\Gamma}}}\sqrt{2M[(1-\kappa)y_{*0}-\lambda_{\rm G}]}$$
$$\times\int_0^{\hat{\xi}_*}\frac{[1+\hat{\eta'}_{\rm T}^2(\hat{\xi}_1)]^{\frac{1}{4}}\hat{\xi}_1^{\frac{1}{2}}}{[1-\alpha_4\hat{B}_0(\hat{\xi}_1)]^{\frac{1}{2}}[\hat{\eta}_{\rm T}^2(\hat{\xi}_1)+\hat{\xi}_1^2]^{\frac{3}{4}}}{\rm d}\hat{\xi}_1$$
$$(n=0,1,2,\cdots), \tag{35}$$

其中

$$\hat{\chi}(\hat{\xi})=\int_{\hat{\xi}_*}^{\hat{\xi}}(1+{\rm i})(1+\hat{\eta'}_{\rm T}^2)^{\frac{1}{4}}$$
$$\times W\sqrt{M\hat{G}\hat{Y}_{\hat{\xi}_1}\frac{(1-\kappa)y_{*0}-\lambda_{\rm G}}{2(1-\alpha_4\hat{B}_0)}}{\rm d}\hat{\xi}_1,$$

$$\Delta(\varepsilon)=\exp\left\{\frac{-(1-i)}{\sqrt{\varepsilon\hat{\Gamma}}}\frac{W(1-\lambda_0)}{\pi}\times\sqrt{2M[(1-\kappa)y_{*0}-\lambda_{\rm G}]}\times\int_{\hat{\xi}_*}^{\frac{1}{\delta(\varepsilon)}}\frac{[1+\hat{\eta}'^2_{\rm T}(\hat{\xi}_1)]^{\frac{1}{4}}\hat{\xi}_1^{\frac{1}{2}}}{[1-\alpha_4\hat{B}_0(\hat{\xi}_1)]^{\frac{1}{2}}[\hat{\eta}^2_{\rm T}(\hat{\xi}_1)+\hat{\xi}_1^2]^{\frac{3}{4}}}{\rm d}\hat{\xi}_1\right\},$$

$q_0=0.412804,\quad q_1=3.143453,$

$q_2=6.283189,\quad q_3=9.424778,\quad\cdots.$

由量子化条件(35)可知, 每给定一个$q_n(n=0,1,2,\cdots)$, 可以解出相应的满足量子化条件的特征值$\hat{\xi}_*=\{\hat{\xi}_*^{(0)},\hat{\xi}_*^{(1)},\hat{\xi}_*^{(2)},\cdots\}$, 它们是参数$\varepsilon$和其他参数的函数, 并且$\hat{\xi}_*^{(0)}<\hat{\xi}_*^{(1)}<\hat{\xi}_*^{(2)}<\cdots$. 计算结果表明, 特征值随着$n$增大而增大, 所以只取最小的特征值$\hat{\xi}_*^{(0)}$. 当$q_0$给定时, 可以得到参数$\varepsilon$与其他参数之间的关系, 再固定除$\hat{\xi}_*^{(0)}$以外的参数, 通过改变参数$\varepsilon$的取值, 可以得到参数$\varepsilon$与特征值$\hat{\xi}_*^{(0)}$的关系, 即图1和图2. 从图1中可以看出, 当两个各向异性偏好方向之间相差的角度θ_0为0时, $\hat{\xi}_*^{(0)}$随着各向异性表面张力系数α_4的增大而减小, 在低阶时与各向异性界面动力学无关. 从图2中可以看出, 当$0\leqslant\theta_0\leqslant\pi/4$时, $\hat{\xi}_*^{(0)}$随着θ_0的增大而增大; 当$\pi/4\leqslant\theta_0\leqslant\pi/2$时, , $\hat{\xi}_*^{(0)}$随着θ_0的增大而减小.

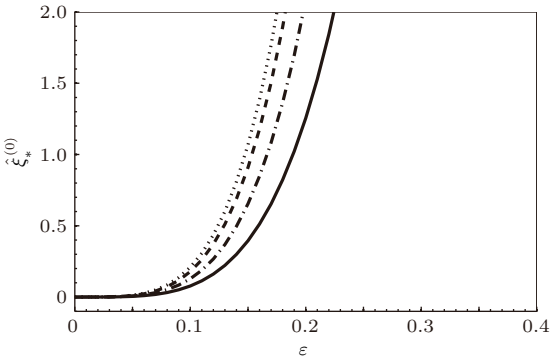

图1 特征值$\hat{\xi}_*^{(0)}$在不同表面张力系数α_4下随ε的变换 参数取值为$\kappa=0.1$, $\lambda_{\rm G}=2$, $\lambda_0=0.6$, $M=1$, $c_0=2.63$, $c=0.88$, $\hat{\Gamma}=1$, $\theta_0=0$, 曲线从左到右分别对应$\alpha_4=0,0.01,0.03,0.06$

Fig. 1. The variations of $\hat{\xi}_*^{(0)}$ with the parameter ε for the cases: $\kappa=0.1$, $\lambda_{\rm G}=2$, $\lambda_0=0.6$, $M=1$, $c_0=2.63$, $c=0.88$, $\hat{\Gamma}=1$, $\theta_0=0$, and $\alpha_4=0,0.01,0.03,0.06$ from left to right.

当$\hat{\xi}_*$确定时, 参数$\hat{\eta}_*$, $\hat{\eta}_{\rm b}$和整个区域$(0\leqslant\hat{\xi}<\infty)$内的内解都会随之确定. 将内解(34)和外解(17)进行匹配, 得到界面形状的合成解为

$$\eta_{\rm B}(\xi,\varepsilon)=\delta(\varepsilon)\hat{\eta}_{\rm T}(\hat{\xi})-\varepsilon c_0(1+\xi)^{\rm c}+\varepsilon h_1(\xi)-\varepsilon h_1(0)\left[{\rm e}^{\frac{\chi_{\rm I}(\xi)}{\sqrt{\varepsilon\hat{\Gamma}}}}\cos\frac{\chi_{\rm R}(\xi)}{\sqrt{\varepsilon\hat{\Gamma}}}+\Delta(\varepsilon)\,{\rm e}^{\frac{\hat{\chi}_{\rm I}(\hat{\xi})}{\sqrt{\varepsilon\hat{\Gamma}}}}\cos\left(\frac{\hat{\chi}_{\rm R}(\hat{\xi})}{\sqrt{\varepsilon\hat{\Gamma}}}\right)\right]+\cdots. \tag{36}$$

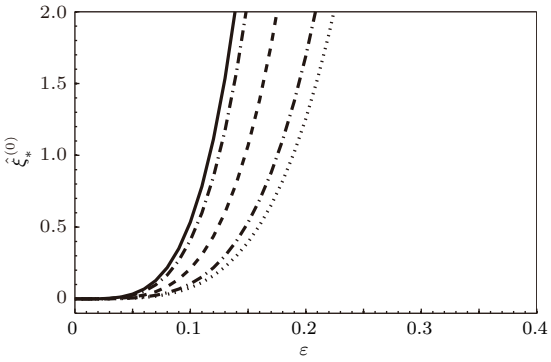

图2 特征值$\hat{\xi}_*^{(0)}$在不同表面张力系数α_4下随ε的变换 参数取值为$\kappa=0.1$, $\lambda_{\rm G}=2$, $\lambda_0=0.6$, $M=1$, $c_0=2.63$, $c=0.88$, $\hat{\Gamma}=1$, $\alpha_4=0.06$, 曲线从左到右分别对应$\theta_0=\frac{4}{16}\pi$, $\frac{3}{16}\pi$或$\frac{5}{16}\pi$, $\frac{2}{16}\pi$或$\frac{6}{16}\pi$, $\frac{1}{16}\pi$或$\frac{7}{16}\pi$, 0或$\frac{8}{16}\pi$

Fig. 2. The variations of $\hat{\xi}_*^{(0)}$ with the parameter ε for the cases: $\kappa=0.1$, $\lambda_{\rm G}=2$, $\lambda_0=0.6$, $M=1$, $c_0=2.63$, $c=0.88$, $\hat{\Gamma}=1$, $\alpha_4=0.06$, and $\theta_0=\frac{4}{16}\pi$, $\frac{3}{16}\pi$ or $\frac{5}{16}\pi$, $\frac{2}{16}\pi$ or $\frac{6}{16}\pi$, $\frac{1}{16}\pi$ or $\frac{7}{16}\pi$, 0 or $\frac{8}{16}\pi$ from left to right.

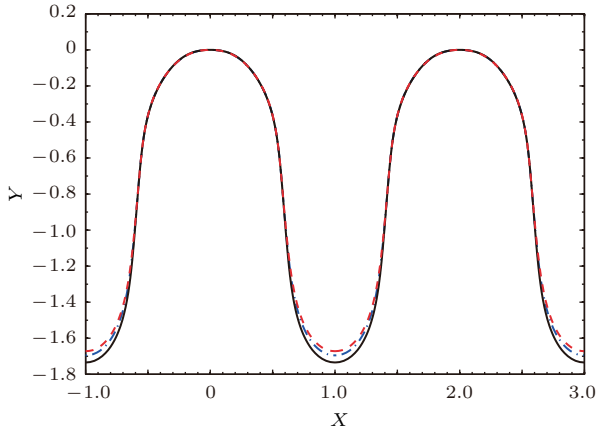

图3 深胞晶界面形状合成解函数$\eta_{\rm B}$在(X,Y)平面内的界面形状 参数取值为$\kappa=0.1$, $\lambda_{\rm G}=2$, $\lambda_0=0.6$, $M=1$, $c_0=2.63$, $c=0.88$, $E=0.5$, $\hat{\Gamma}=1$, $m_*=1$, $\beta_4=0.03$, $\theta_0=0$, 从上到下的三条曲线分别对应$\alpha_4=0.01,0.03,0.06$

Fig. 3. The composite solution for the interface shape function $\eta_{\rm B}$ described on (X,Y) plane for the case: $\kappa=0.1$, $\lambda_{\rm G}=2$, $\lambda_0=0.6$, $M=1$, $c_0=2.63$, $c=0.88$, $E=0.5$, $\hat{\Gamma}=1$, $m_*=1$, $\beta_4=0.03$, $\theta_0=0$, and different values of the anisotropic surface-tension coefficient $\alpha_4=0.01,0.03,0.06$ from top to bottom.

由界面形状的合成解(36)式可知, 当参数取值固定时, 可以得到深胞晶界面形状合成解函数$\eta_{\rm B}$在(X,Y)平面内的界面形状, 即图3、图4和图5.

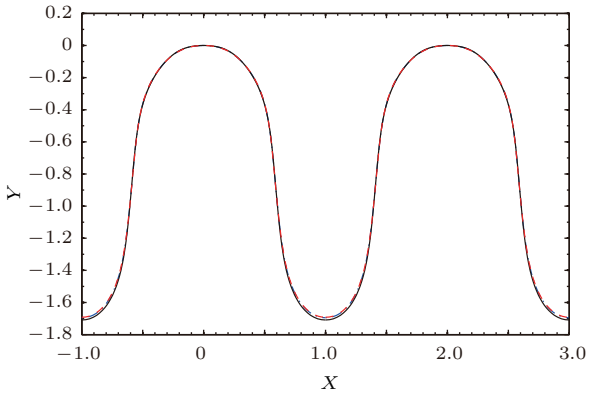

图4 深胞晶界面形状合成解函数$\eta_{\rm B}$在(X,Y)平面内的界面形状 参数取值为$\kappa=0.1$, $\lambda_{\rm G}=2$, $\lambda_0=0.6$, $M=1$, $c_0=2.63$, $c=0.88$, $E=0.5$, $\hat{\Gamma}=1$, $m_*=1$, $\alpha_4=0.03$, $\theta_0=0$, 从上到下的三条曲线分别对应$\beta_4=0.01,0.03,0.06$

Fig. 4. The composite solution for the interface shape function $\eta_{\rm B}$ described on (X,Y) plane for the case: $\kappa=0.1$, $\lambda_{\rm G}=2$, $\lambda_0=0.6$, $M=1$, $c_0=2.63$, $c=0.88$, $E=0.5$, $\hat{\Gamma}=1$, $m_*=1$, $\alpha_4=0.03$, $\theta_0=0$, and different values of the anisotropic interface kinetics coefficient $\beta_4=0.01,0.03,0.06$ from top to bottom.

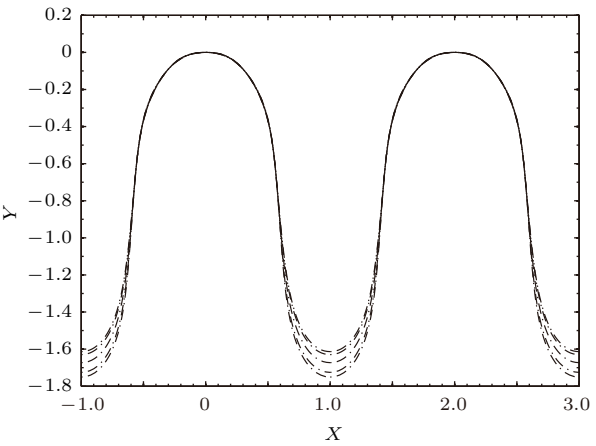

图5 深胞晶界面形状合成解函数$\eta_{\rm B}$在(X,Y)平面内的界面形状 参数取值为$\kappa=0.1$, $\lambda_{\rm G}=2$, $\lambda_0=0.6$, $M=1$, $c_0=2.63$, $c=0.88$, $E=0.5$, $\hat{\Gamma}=1$, $m_*=1$, $\alpha_4=0.06$, $\beta_4=0.06$, 从上到下的五条曲线分别对应$\theta_0=\frac{4}{16}\pi$, $\frac{3}{16}\pi$或$\frac{5}{16}\pi$, $\frac{2}{16}\pi$或$\frac{6}{16}\pi$, $\frac{1}{16}\pi$或$\frac{7}{16}\pi$, 0或$\frac{8}{16}\pi$

Fig. 5. The composite solution for the interface shape function $\eta_{\rm B}$ described on (X,Y) plane for the case: $\kappa=0.1$, $\lambda_{\rm G}=2$, $\lambda_0=0.6$, $M=1$, $c_0=2.63$, $c=0.88$, $E=0.5$, $\hat{\Gamma}=1$, $m_*=1$, $\alpha_4=0.06$, $\beta_4=0.06$, and different values of the angle $\theta_0=\frac{4}{16}\pi$, $\frac{3}{16}\pi$ or $\frac{5}{16}\pi$, $\frac{2}{16}\pi$ or $\frac{6}{16}\pi$, $\frac{1}{16}\pi$ or $\frac{7}{16}\pi$, 0 or $\frac{8}{16}\pi$ from top to bottom.

从图3和图4中可以看出, 当两个各向异性偏好方向之间相差的角度θ_0为0时, 随着各向异性系数的增大, 深胞晶的指状界面全长增大, 根部底端的曲率半径会减小, 即根部底端的曲率增大, 在同一数量级下, 各向异性表面张力系数对界面形状的影响更为显著. 从图5中可以看出, 当$0\leqslant\theta_0\leqslant\pi/4$时, 随着$\theta_0$增大, 深胞晶的指状界面全长减小, 根部底端的曲率半径会减小, 即根部底端的曲率增大; 当$\pi/4\leqslant\theta_0\leqslant\pi/2$时, 随着$\theta_0$增大, 深胞晶的指状界面全长增大, 根部底端的曲率半径会增大, 即根部底端的曲率减少. 各向异性和角度θ_0对深胞晶的总长度和根部均有显著影响, 但在其他固-液界面上, 比如深胞晶的顶部, 所起的作用并不大.

5 结 论

本文应用配渐近展开法和多重变量渐近展开法研究了定向凝固过程中各向异性界面动力学与各向异性表面张力的相互作用对深胞晶生长界面形态的影响, 分析了当各向异性界面动力学与各向异性表面张力的偏好方向之间相差角度为θ_0时稳定态的特征值问题. 结果表明, 各向异性界面动力学与各向异性表面张力的偏好方向之间相差的角度会对深胞晶生长形态产生影响. 当两种各向异性偏好方向相同, 即θ_0为0时, 随着各向异性系数的增大, 深胞晶的指状界面全长增大, 根部底端的曲率半径会减小, 即根部底端的曲率增大, 且各向异性表面张力系数对深胞晶生长界面形状的影响更为显著. 当$0\leqslant\theta_0\leqslant\pi/4$时, 随着$\theta_0$增大, 深胞晶的指状界面全长减小, 根部底端的曲率半径会减小, 即根部底端的曲率增大; 当$\pi/4\leqslant\theta_0\leqslant\pi/2$时, 随着$\theta_0$增大, 深胞晶的指状界面全长增大, 根部底端的曲率半径会增大, 即根部底端的曲率减少.

参考文献

[1] Ding G L, Huang W D, Lin X, Zhou Y 1997 *J. Cryst. Growth* **177** 281
[2] Ding G L, Lin H, Huang W D, Zhou Y H 1995 *Acta Metall. Sin.* **31** 469
[3] Georgelin M, Pocheau A 2006 *Phys. Rev. E* **73** 011604
[4] Georgelin M, Pocheau A 2009 *Phys. Rev. E* **81** 031601
[5] Chen Y Q, Xu J J 2011 *Phys. Rev. E* **83** 041601
[6] Xu J J, Chen Y Q 2015 *Eur. J. Appl. Math.* **26** 1
[7] Mullins W W, Sekerka R F 1963 *J. Appl. Phys.* **34** 323
[8] Mullins W W, Sekerka R F 1964 *J. Appl. Phys.* **35** 444

[9] Saffman P G, Taylor G I 1958 *Proc. R. Soc. London A* **245** 312
[10] Coriell S R, Sekerka R F 1976 *J. Cryst. Growth* **34** 157
[11] Wang Z J, Wang J C, Yang G C 2008 *Acta Phys. Sin.* **57** 1246 (in Chinese) [王志军, 王锦程, 杨根仓 2008 物理学报 **57** 1246]
[12] Wang Z J, Wang J C, Yang G C 2010 *Chin. Phys. B* **19** 017305
[13] Trivedi R, Seetharaman V, Eshelman M A 1991 *Mater. Trans. A* **22** 585
[14] Chen M W, Chen Y C, Zhang W L, Liu X M, Wang Z D 2014 *Acta Phys. Sin.* **63** 038101 (in Chinese) [陈明文, 陈奕臣, 张文龙, 刘秀敏, 王自东 2014 物理学报 **63** 038101]
[15] Jiang H, Chen M W, Shi G D, Wang T, Wang Z D 2016 *Mod. Phys. Lett. B* **30** 1650205
[16] Ihle T 2000 *Eur. Phys. J. B* **16** 337

Effects of anisotropic interface kinetics and surface tension on deep cellular crystal growth in directional solidification

Jiang Han[1)] Chen Ming-Wen[2)†] Wang Tao[1)] Wang Zi-Dong[1)‡]

1) (*School of Materials Science and Engineering, University of Science and Technology Beijing, Beijing 100083, China*)

2) (*School of Mathematics and Physics, University of Science and Technology Beijing, Beijing 100083, China*)

(Received 5 January 2017; revised manuscript received 26 February 2017)

Abstract

In this paper, we study the effects of anisotropic interface kinetics and surface tension on deep cellular crystal growth in directional solidification. The following assumptions are made: the process of solidification is viewed as a two-dimensional problem; the minor species in this binary mixture system is considered as an impurity; the solute diffusion in the solid phase is negligible; the thermodynamic properties other than the diffusivities are the same for both solid and liquid phases; there is no convection in the system; the anisotropic interface kinetics and the anisotropic surface tension are a four-fold symmetry function each; neither the preferred directions of the anisotropic interface kinetics nor the anisotropic surface tensions are necessarily the same as their counterparts for the solid and liquid phases respectively; the angle between the preferred directions of the two anisotropies is θ_0. By using the matched asymptotic expansion method and the multiple variable expansion method, we obtain the diagram of interface morphology for a deep cellular crystal in directional solidification.

The results show that there exists a discrete set of the steady-state solutions subject to the quantization condition (35). The quantization condition yields the eigenvalue $\hat{\xi}_*$ as a function of parameter ε and other parameters of the system, which determines the interface morphology of the cell. The results also show the variation of the minimum eigenvalue $\hat{\xi}_*^{(0)}$ with parameter ε. It is seen that when the preferred directions of the two anisotropies are the same, i.e., $\theta_0 = 0$, the minimum eigenvalue $\hat{\xi}_*^{(0)}$ reduces with the increase of anisotropic surface-tension coefficient α_4, increases with the augment of parameter ε, and is unrelated to anisotropic interface kinetic coefficient β_4 in the low order; when the angle $0 \leqslant \theta_0 \leqslant \pi/4$, as the θ_0 increases, the minimum eigenvalue $\hat{\xi}_*^{(0)}$ increases; when the angle $\pi/4 \leqslant \theta_0 \leqslant \pi/2$, as the θ_0 increases, the minimum eigenvalue $\hat{\xi}_*^{(0)}$ decreases. In addition, the results show the composite solution for the interface shape function $\eta_{\rm B}$ described on (X, Y) plane. It is seen that both of the anisotropy and the angle θ_0 have a significant effect on the total length and the root of deep cellular crystal, however, have little influence on the other solid-liquid interface, such as the top of deep cellular crystal. When the angle θ_0 is 0, as anisotropic coefficient increases, the total length of the finger increases, the curvature of the interface near the root increases or the curvature radius decreases. It is found that the influence of the anisotropic surface-tension coefficient on interface morphology is more remarkable than that of the anisotropic interface kinetics coefficient. when the angle $0 \leqslant \theta_0 \leqslant \pi/4$, as the θ_0 increases, the total length of the finger decreases, the curvature of the interface near the root decreases or the curvature radius increases; when the angle $\pi/4 \leqslant \theta_0 \leqslant \pi/2$, as θ_0 increases, the total length of the finger increases, the curvature of the interface near the root increases or the curvature radius decreases.

Keywords: directional solidification, anisotropic surface tension, anisotropic interface kinetics, deep cellular crystal growth

PACS: 68.70.+w, 81.10.Aj, 81.30.Fb **DOI:** 10.7498/aps.66.106801

† Corresponding author. E-mail: chenmw@ustb.edu.cn

‡ Corresponding author. E-mail: wangzd@mater.ustb.edu.cn